

Detections of simultaneous brightening of γ -ray and optical emissions of a high-redshift blazar
GB 1508+5714

NENG-HUI LIAO,¹ SHANG LI,² AND YI-ZHONG FAN²

¹*Department of Physics and Astronomy, College of Physics, Guizhou University, Guiyang 550025, China*

²*Key Laboratory of Dark Matter and Space Astronomy, Purple Mountain Observatory, Chinese Academy of Sciences, Nanjing 210034, China*

ABSTRACT

GB 1508+5714 is a high-redshift blazar ($z = 4.3$) and a spectrally soft γ -ray source has been found in its direction. By analyzing 11.4-yr *Fermi*-LAT data, significant long-term variability of the γ -ray source is confirmed. More importantly, a γ -ray emission flare appeared in an epoch of several tens of days in year 2018, when the flux is about four times of the value from the global fit. Meanwhile, optical flares displayed in both *i*- and *r*-bands from the *Zwicky* Transient Facility light curves. Detections of the simultaneous γ -ray and optical brightening provide a decisive proof to pin down the association between the γ -ray source and GB 1508+5714, which makes it the *first* identified γ -ray blazar beyond redshift 4. Future multiwavelength campaigns are needed to further investigate its jet properties, and, upcoming wide-deep-fast optical telescopes together with the γ -ray sky surveyors will shed lights on the role that the AGN jets play in the early cosmic time.

Keywords: galaxies: active – galaxies: high-redshift – galaxies: jets – gamma rays:
galaxies – quasars: individual (GB 1508+5714)

1. INTRODUCTION

Benefited from the strongly boosted jet emission (Blandford & Rees 1978; Blandford et al. 2019), blazars are bright beacons (e.g., Ghisellini et al. 2014b) and capable to be detected even in the early cosmic time (e.g., Romani et al. 2004; Romani 2006). High-redshift blazars are valuable targets for understanding the formation and growth of the first generation of super massive black holes as well as the cosmic evolution of AGN jets (Ghisellini et al. 2010; Volonteri 2010). Meanwhile, their emissions carry crucial information of the early universe. Particularly, the γ -ray emission of high-redshift blazars is valuable for probing the extragalactic background light (EBL, e.g., *Fermi*-LAT Collaboration et al. 2018). However, as a result of the faintness due to their large distances, the number of detected high-redshift (i.e. $z > 4$) blazars (candidates) is limited (Massaro et al. 2009). In fact, it becomes rather challenging in the γ -ray domain. In the fourth *Fermi* Large Area Telescope (LAT, Atwood et al. 2009) catalog (4FGL, Abdollahi et al. 2020), all blazars beyond redshift 3 are flat-spectrum radio

quasars (FSRQs). Since the peak of their high energy spectral energy distribution (SED) bump is beneath the lower energy threshold of *Fermi*-LAT, the decline of γ -ray emissions caused by the significant cosmic redshift is a major obstacle for γ -ray blazar detection at high redshifts.

Blazars are characterized by violent multiwavelength variability (e.g., Ulrich et al. 1997; Madejski & Sikora 2016). Coincidences between their γ -ray flares and ones in other windows of electromagnetic radiation have been frequently detected (e.g., Abdo et al. 2010; Liao et al. 2014). In the perspective of the relatively limited angular resolution of the γ -ray observation, catching these correlated variations provide a decisive proof to support the association between the γ -ray source and its low-energy counterpart (e.g., Schinzel et al. 2011; Liao et al. 2016). In the high-redshift regime, based on the strong quasi-simultaneous IR and γ -ray flares, CGRaBS J0733+0456 ($z = 3.01$) is proved to an identified γ -ray source (Liao et al. 2019). GB 1508+5714 was initially detected as a radio source at 5 GHz (Patnaik et al. 1992) and then identified as a high-redshift quasar ($z = 4.3$, Hook et al. 1995). Considering the flat radio spectrum and the high radio loudness (Kellermann et al. 1989) value, as well as the hard X-ray spectrum (Mathur & Elvis 1995; Moran & Helfand 1997), it has been suggested to be a blazar (Massaro et al. 2009). More importantly, a faint and spectrally soft γ -ray source (categorized as 4FGL J1510.1+5702 in 4FGL, Abdollahi et al. 2020) cospatial with GB 1508+5714 is found and hence it is claimed as the most distant γ -ray blazar so far (Ackermann et al. 2017). By analyzing nearly the first 9 years *Fermi*-LAT data, the γ -ray source towards GB 1508+5714 is suggested to be likely variable (Li et al. 2018). Meanwhile, its overall broadband SED is similar with those of γ -ray FSRQs, further supporting its blazar nature (Marcotulli et al. 2020). However, due to the faintness and the soft γ -ray spectrum, and considering that the angular resolution of *Fermi*-LAT for sub-GeV photons is much worse than for GeV γ rays¹, its nature of γ -ray blazar can not be set in stone until detections of multiwavelength correlated variations.

In this letter, we analyze the 11.4-yr of *Fermi*-LAT data as well as the Intermediate Palomar Transient Factory (iPTF) and *Zwicky* Transient Facility (ZTF) light curve data of GB 1508+5714, and investigate its multiwavelength variability properties (Section 2), along with some discussions (Section 3). Here we take a Λ CDM cosmology with $H_0 = 67 \text{ km s}^{-1} \text{ Mpc}^{-1}$, $\Omega_m = 0.32$, and $\Omega_\Lambda = 0.68$ (Planck Collaboration et al. 2014).

2. DATA ANALYSIS AND RESULTS

2.1. *Fermi*-LAT data

Here the *Fermi*-LAT Pass 8 SOURCE data (from MJD 54682 to MJD 58852) with energy range between 100 MeV and 500 GeV are collected and analyzed by the `Fermitools` software version 1.2.23. The entire data set is filtered with the zenith angle cut ($< 90^\circ$) as well as the recommended quality-filter cuts (`DATA_QUAL==1 && LAT_CONFIG==1`). Unbinned likelihood analyses implemented in the `gtlike` task is used to extract the γ -ray flux and spectrum. The initial background model includes all 4FGL sources within 15° around 4FGL J1510.1+5702, together with the diffuse γ -ray emission templates (i.e. `gll_iem_v07.fits` and `iso_P8R3_SOURCE_V2_v1.txt`). During the likelihood analyses, parameters of all 4FGL sources lying within a 10° region of interest centered at the location of 4FGL J1510.1+5702, as well as the normalizations of the two diffuse emission backgrounds are set free. The significance of a γ -ray source is quantified by the test statistic (TS, Mattox et al. 1996),

¹ http://www.slac.stanford.edu/exp/glast/groups/candalat_Performance.htm

which is defined as $TS = -2\ln(L_0/L)$ where L and L_0 are the maximum likelihood values for the model with and without target source, respectively. In the temporal analysis, the spectral parameters of background sources are frozen with the values from the global fit, unless they are bright or close to the target. Meanwhile, the faint ($TS < 10$) background sources are removed from the model and then the likelihood analyses are performed again. If TS value of the target is lower than 10, the 95% confidential level (C.L.) upper limit is calculated by the `pyLikelihood UpperLimits` tool instead of estimating the flux.

The analysis of the entire 11.4-yr of *Fermi*-LAT data yields a significant γ -ray source in the direction of GB 1508+5714. The γ -ray source has a rather soft spectrum, $dN/dE \propto E^{-(3.05 \pm 0.15)}$, consistent with the result from 4FGL (Abdollahi et al. 2020). The radio location of GB 1508+5714 remains to be within the γ -ray 95% C.L. error radius. Moreover, the TS value ($TS = 78, 8.1\sigma$) is doubled compared with it from 4FGL ($TS = 37, 5.2\sigma$, Abdollahi et al. 2020²). The significantly enhanced TS value suggests that a rise of the γ -ray emission likely appears after the first 8-year *Fermi*-LAT operation. Therefore, an individual analysis focusing on the last 3.4-yr *Fermi*-LAT data has been performed, and we find a robust γ -ray source ($TS = 41, 5.6\sigma$), as shown in Figure 1. Its spectral index is constrained as 2.94 ± 0.18 . Localization analysis gives an optimum location of R.A. 227.65° and DEC. 57.182° with a 95% C. L. error radius of 0.25° , which overlaps with the radio location of GB 1508+5714. And there is no other blazars (candidates) (e.g., Healey et al. 2008; Massaro et al. 2009) in such a region. We have checked whether there are new γ -ray sources (i.e. not included in 4FGL) close to 4FGL J1510.1+5702 emerging recently. In a short period, from 9th July 2018 to Oct. 7th 2018, a new γ -ray source with TS value of 34 just 0.5° away from the radio position of GB 1508+5714 appeared. Its optimum location is R.A. 226.755° and DEC. 57.336° , with a 95% C. L. error radius of 0.3° , might associate with a radio source NVSS J150754+571723. After extracting this source, no significant γ -ray residual is found towards GB 1508+5714 then. In consideration of the proximity, *Fermi*-LAT data during such a 3-month epoch are eliminated during the entire and the last 3.4-yr *Fermi*-LAT data analyses.

Then a 3-month time bin light curve is extracted to investigate the γ -ray temporal properties, see Figure 2. In most cases, the γ -ray source is not well distinguished from the background (i.e. $TS \leq 20$), which is agreed with the literature (Li et al. 2018). However, one time bin (i.e. from MJD 58217 to MJD 58308) stands out with a $TS \sim 30$. We note that rising of TS value of the target could be caused by flaring of the bright neighbors. Therefore, light curves of two nearby strong background γ -ray sources, 4FGL J1454.4+5124 and 4FGL J1543.0+6130 (both 6° away) whose TS values from the global fit are 8000 and 19000 respectively, are also extracted. Luckily, in this special epoch, no coincident γ -ray flares from the neighbors are found, also see Figure 2. A residual TS map confirms the emergence of a valid γ -ray source towards GB 1508+5714 then, see Figure 1. The optimum location of this source is constrained as R.A. 227.368° and DEC. 57.111° with a 95% C. L. error radius of 0.3° that embraces the radio position of GB 1508+5714. The source is spectrally soft, $\Gamma = 2.97 \pm 0.25$, and no significant spectral hardening is found compared with the global fit. But the flux then, $(3.4 \pm 0.8) \times 10^{-8}$ ph cm⁻² s⁻¹, is roughly four times of the 11.4-yr averaged value, $(7.6 \pm 1.2) \times 10^{-9}$ ph cm⁻² s⁻¹. Due to the limited statistics, it is impossible to obtain any variability information at timescale of a few days. Nevertheless, if the time range of the data narrows down

² Note in 4FGL the summed-binned-likelihood analysis thread is adopted and the energy range of the selected *Fermi*-LAT data there is between 50 MeV and 100 GeV.

to about 48 days (i.e. from MJD 58241 to MJD 58290), TS value of the source is still as large as 26. We also calculate the variability index (Nolan et al. 2012) value based on the 3-month time bin light curve here. The σ_{var} increases from 3.0 (Li et al. 2018) to 4.3 after embracing the latest 2.4-yr *Fermi*-LAT data.

2.2. *i*PTF and ZTF light curve data

Here we adopt the light curve data archived by the IRSA³ from both iPTF and ZTF which use the 48 inch Schmidt telescope at the Palomar Observatory. The total field of view of iPTF is 7.26 deg² and the depth of a single snapshot is $R \simeq 20.5$ mag or $g \simeq 21$ mag when the exposure time is 60 sec under the median seeing (i.e. 2'') (Cao et al. 2016). In 2017, iPTF have transitioned to ZTF which has an enhanced 47 deg² field and scans the northern sky at rates of ~ 3760 deg² per hour (Bellm et al. 2019; Masci et al. 2019; Graham et al. 2019). With exposures in 30 sec, the median depths are $g \sim 20.8$ mag and $r \sim 20.6$ mag (AB, 5 σ). Additionally, *i*-band observations are also carried out in ZTF.

Recently, the second ZTF public data release (DR2) have been announced⁴. Initially, we have looked up the co-added reference images. GB 1508+5714 is faint in the *g*-band image ($\simeq 22.1$ mag, Schneider et al. 2005) but significantly detected in the frames of the rest two filters. Therefore, light curves in *r*-band and *i*-band for objects falling within a 5'' radius from position of the target are derived. There are in total 14 *i*-band exposures (in 13 days from MJD 58227 to MJD 58290) and 252 *r*-band exposures (in 104 days from MJD 58200 to MJD 58660). Only ZTF frames satisfied with `catflags = 0` are selected. In addition, there are 160 *R*-band iPTF exposures (in 65 days from MJD 56008 to MJD 56825). Note that photometric zero-point corrections have been applied for the ZTF and iPTF light curves. The long-term daily averaged optical light curves are shown in Figure 3. The typical mag of GB 1508+5714 for each single ZTF *r*-band exposure is ~ 20 mag. But generally, the *r*-band flux density in year 2018 ($r_{mean} \simeq 20$ mag) appears to be slightly higher than that in year 2019 ($r_{mean} \simeq 20.2$ mag). One attractive feature in the *r*-band light curve is the existence of flares in June 2018. There is a 0.5 mag flux density increase from MJD 58282.2 ($r = 20.0 \pm 0.12$ mag) to MJD 58285.3 ($r = 19.5 \pm 0.08$ mag), and the flux density declines in 4 days ($r = 20.1 \pm 0.13$ mag at MJD 58289.2). Before this major flare, there is a minor flare peaking at MJD 58279.3 with brightening of about 0.3 mag. On the other hand, though the *i*-band light curve is sparsely sampled, the flux density at MJD 58286.3 reached to $i = 18.9 \pm 0.08$ mag, which is significantly brighter than that in MJD 58272.4 ($i = 19.7 \pm 0.13$ mag). The simultaneous brightening of fluxes in the two independent optical bands suggests that GB 1508+571 was indeed undergoing an active phase then. For the iPTF *R*-band light curve, as discussed in Li et al. (2018), no significant optical variability is found there. Besides the daily optical light curves, a zoom of the ZTF light curves in year 2018 with each exposure exhibited is also shown, together with the corresponding airmass and the limit mag, see Figure 4. Considering the limit mag during the optical flare epoch is $i_{limit} \simeq 20.6$ mag/ $r_{limit} \simeq 21.3$ mag, the observations were not carried out in the bad weather condition. Meanwhile, the airmasses then were less than 1.3. Therefore, the optical flares are robust.

2.3. Implications of γ -ray and optical variability

³ <https://irsa.ipac.caltech.edu>

⁴ <https://www.ztf.caltech.edu/news/public-data-release-2>

Our *Fermi*-LAT data analyses reveal that 4FGL J1510.1+5702 is at high flux state in an epoch of several tens of days in year 2018. Interestingly, optical flux densities of GB 1508+5714 in two bands rise in the same epoch, see Figure 3. Such optical variations are likely from the jet because of the large variability amplitude. Based on the simultaneous γ -ray and optical brightening, we conclude that 4FGL J1510.1+5702 is the γ -ray counterpart of GB 1508+5714. There are other three time bins in the γ -ray light curve that the TS values reaches to ≥ 10 . However, unfortunately, no iPTF/ZTF data of GB 1508+5714 then are available. Theoretically, in the leptonic radiation scenario, the optical and GeV γ -ray emissions of low synchrotron peaked blazars, including FSRQs, are proposed to be from the same population of emitting electrons. It is supported by correlated optical/ γ -ray flares in FSRQs (e.g., [Abdo et al. 2010](#); [Bonning et al. 2012](#)). Meanwhile, the redder-when-brighter spectral variability behavior has been detected in the optical wavelengths of γ -ray FSRQs, which is explained by the influence of the blue and slowly varying accretion disk emission (e.g., [Bonning et al. 2012](#)). For GB 1508+5714, a similar trend is shown. The optical spectral color, $r-i$, is 0.66 mag in MJD 58286, while it is 0.43 mag in MJD 58272, despite the relatively large photometric uncertainties. And its i -band variability amplitude is higher than that in r -band. Though the statistic of the γ rays is limited, the variability timescale in the source frame can be constrained as short as ~ 0.9 day, based on the rapid r -band flux density ascent before MJD 58285.3. Assuming that optical and γ -ray photons of GB 1508+5714 are from the same compact region, the Doppler factor should be high enough to avoid serious absorption of γ rays via the $\gamma\gamma$ process ([Dondi & Ghisellini 1995](#); [Begelman et al. 2008](#)). Since the highest energy of the detected γ -ray photons is ~ 8 GeV, if the soft photons from jet itself (detected at a few keVs, 3×10^{46} erg s $^{-1}$, [Marcotulli et al. 2020](#)) is responsible for the absorption, a constraint of $\delta \gtrsim 7$ is given.

3. DISCUSSIONS AND SUMMARY

Activity of γ -ray emissions of high-redshift ($z \geq 2$) blazars is intense. Their peaking γ -ray luminosity is capable to reach to $> 10^{50}$ erg s $^{-1}$ ([Abdo et al. 2015](#); [D'Ammando & Orienti 2016](#)). Meanwhile, the variability amplitude can be as high as over one order of magnitude and the timescale of fast variations down to a few hours in the source frame have been often detected (e.g., [Akyuz et al. 2013](#); [Abdo et al. 2015](#); [Li et al. 2018](#)). By comparison, the γ -ray variation of GB 1508+5714 appears to be mild and the peaking luminosity is 2×10^{48} erg s $^{-1}$. Nevertheless, intraday optical variation of GB 1508+5714 is detected during the γ -ray brightening epoch. Considering intraday variability at optical/IR wavelengths detected in other high-redshift γ -ray blazars (e.g., [Li et al. 2018](#); [Liao et al. 2019](#)), it is reasonable that highly beamed sources are more likely to be seen there due to the Malmquist bias. More importantly, the simultaneous brightening in optical (both in r - and i -bands) as well as γ rays, provides the crucial evidence for GB 1508+5714 being a γ -ray emitter. GB 1508+5714 is a very important target for future multiwavelength campaign to probe the jet properties at high redshifts. It is worthwhile to note that there is another interesting source, NVSS J163547+362930 ($z = 3.6$, [Pâris et al. 2014](#)), from which detections of significant optical and γ -ray flares, though not simultaneously, have been reported ([Li et al. 2018](#)).

Besides blazars, γ -ray bursts (GRBs) are also strong extragalactic γ -ray emitters. The most distant GRB with GeV γ -ray detection by *Fermi*-LAT so far is GRB 080916C ($z_{\text{ph}} = 4.35$, [Greiner et al. 2009](#); [Abdo et al. 2009](#)). For blazars, the most distant source in hard X rays among the 105 month Swift-BAT all sky survey ([Oh et al. 2018](#)) is B3 1428+422 ($z = 4.7$, [Hook & McMahon 1998](#)). Meanwhile, individual studies reveal several blazars (candidates) beyond redshift 5, including Q0906+6930 (z

= 5.48, Romani et al. 2004), SDSS J102623.61+254259.5 ($z = 5.2$, Sbarrato et al. 2012), SDSS J013127.34−032100.1 ($z = 5.18$, Yi et al. 2014, and SDSS J114657.79+403708.6 ($z = 5.0$; Ghisellini et al. 2014a). Attempts that aim to break the redshift record by GRB 080916C have been made. A new spectrally soft transient (in an epoch of 10 months) γ -ray source (global significance of 4.1σ) towards B3 1428+422 is detected by *Fermi*-LAT, despite there is no significant excess there from a entire 9-year data averaged perspective (Liao et al. 2018). Unfortunately, there are no available simultaneous observations that can be used to pin down the relationship between the transient γ -ray source and B3 1428+422. Meanwhile, TS value of one time bin of the γ -ray light curve of Q0906+6930 is about 12, locally $\sim 2\sigma$ (An & Romani 2018). If blazars of $z \gtrsim 5$ are as violently variable as ones of $z \simeq 3$, their γ -ray emissions would be likely detected by *Fermi*-LAT during the flaring epochs. Moreover, the next generation MeV γ -ray all-sky surveyor, like the All sky Medium Energy Gamma-ray Observatory (McEnery & Amego Team 2020), will play an important role of detecting high-redshift blazars. On the other hand, complementary time domain observations in other windows of the electromagnetic radiation are also crucial. Note that the optical emission of blazars at $z \gtrsim 5$ is very faint, for example $R_{\text{Q0906+6930}} = 21.7$ mag (Healey et al. 2008). Upcoming 2-meter class wide-deep-fast optical sky surveyors in the northern hemisphere, like the Wide Field Survey Telescope (Lou et al. 2016), as well as the Large Synoptic Survey Telescope (Ivezić et al. 2019), will bring a bright future of catching activities from the jets in AGNs in the early cosmic time.

In summary, we perform an investigation of the γ -ray and optical variability properties of GB 1508+5714. TS value from the analysis of the entire 11.4-yr *Fermi*-LAT data is doubled compared with the value listed in 4FGL. The γ -ray source is indeed at a high flux state in an epoch of several tens of days in year 2018. The flux then is about four times of the flux from the global fit, and the corresponding TS value reaches to 30. Meanwhile, at the same time, significant rise of the optical fluxes, both in *i*- and *r*-bands, are found through the ZTF light curves. The sign of fast variation in *r*-band and the redder-when-brighter optical spectral variability are also detected then. In consideration of the γ -ray and optical brightening, GB 1508+5714 is strongly suggested to be the *first* identified γ -ray blazar beyond redshift 4. Future multiwavelength campaigns are urged to further investigate its jet properties.

This research has made use of data obtained from the High Energy Astrophysics Science Archive Research Center (HEASARC), provided by NASA’s Goddard Space Flight Center. This research has made use of the NASA/IPAC Infrared Science Archive, which is funded by the NASA and operated by the California Institute of Technology. This study use data based on observations obtained with the Samuel Oschin 48-inch Telescope at the Palomar Observatory as part of the iPTF and ZTF projects. ZTF is supported by the National Science Foundation under Grant No. AST-1440341 and a collaboration including Caltech, IPAC, the Weizmann Institute for Science, the Oskar Klein Center at Stockholm University, the University of Maryland, the University of Washington, Deutsches Elektronen-Synchrotron and Humboldt University, Los Alamos National Laboratories, the TANGO Consortium of Taiwan, the University of Wisconsin at Milwaukee, and Lawrence Berkeley National Laboratories. Operations are conducted by COO, IPAC, and UW.

This work was supported in part by the National Basic Research Program of China (No. 2013CB837000), NSFC under grants 11525313 (i.e., Funds for Distinguished Young Scholars) and 11703093.

REFERENCES

- Abdo, A. A., Ackermann, M., Arimoto, M., et al. 2009, *Science*, 323, 1688
- Abdo, A. A., et al. 2010, *Nature*, 463, 919
- Abdo, A. A., Ackermann, M., Ajello, M., et al. 2015, *ApJ*, 799, 143
- Abdollahi, S., Acero, F., Ackermann, M., et al. 2020, *ApJS*, 247, 33
- Ackermann, M., Ajello, M., Baldini, L., et al. 2017, *ApJL*, 837, L5
- Akyuz, A., Thompson, D. J., Donato, D., et al. 2013, *Astron. Astrophys.*, 556, A71
- An, H., & Romani, R. W. 2018, *ApJ*, 856, 105
- Atwood, W. B., et al. 2009, *Astrophys. J.*, 697, 1071
- Begelman, M. C., Fabian, A. C., & Rees, M. J. 2008, *MNRAS*, 384, L19
- Bellm, E. C., Kulkarni, S. R., Graham, M. J., et al. 2019, *PASP*, 131, 018002
- Blandford, R., Meier, D., & Readhead, A. 2019, *ARA&A*, 57, 467
- Blandford, R. D., & Rees, M. J. 1978, in *BL Lac Objects*, ed. A. M. Wolfe, 328–341
- Bonning, E., Urry, C. M., Bailyn, C., et al. 2012, *ApJ*, 756, 13
- Cao, Y., Nugent, P. E., & Kasliwal, M. M. 2016, *PASP*, 128, 114502
- D’Ammando, F., & Orienti, M. 2016, *MNRAS*, 455, 1881
- Dondi, L., & Ghisellini, G. 1995, *MNRAS*, 273, 583
- Fermi*-LAT Collaboration, Abdollahi, S., Ackermann, M., et al. 2018, *Science*, 362, 1031
- Ghisellini, G., Sbarrato, T., Tagliaferri, G., et al. 2014a, *MNRAS*, 440, L111
- Ghisellini, G., Tavecchio, F., Maraschi, L., Celotti, A., & Sbarrato, T. 2014b, *Nature*, 515, 376
- Ghisellini, G., Della Ceca, R., Volonteri, M., et al. 2010, *MNRAS*, 405, 387
- Graham, M. J., Kulkarni, S. R., Bellm, E. C., et al. 2019, *PASP*, 131, 078001
- Greiner, J., Clemens, C., Krühler, T., et al. 2009, *A&A*, 498, 89
- Healey, S. E., Romani, R. W., Cotter, G., et al. 2008, *ApJS*, 175, 97
- Hook, I. M., & McMahon, R. G. 1998, *MNRAS*, 294, L7
- Hook, I. M., McMahon, R. G., Patnaik, A. R., et al. 1995, *MNRAS*, 273, L63
- Ivezić, Ž., Kahn, S. M., Tyson, J. A., et al. 2019, *ApJ*, 873, 111
- Kellermann, K. I., Sramek, R., Schmidt, M., Shaffer, D. B., & Green, R. 1989, *AJ*, 98, 1195
- Li, S., Xia, Z.-Q., Liang, Y.-F., Liao, N.-H., & Fan, Y.-Z. 2018, *ApJ*, 853, 159
- Liao, N. H., Bai, J. M., Liu, H. T., et al. 2014, *ApJ*, 783, 83
- Liao, N.-H., Dou, L.-M., Jiang, N., et al. 2019, *ApJL*, 879, L9
- Liao, N.-H., Li, S., & Fan, Y.-Z. 2018, *ApJL*, 865, L17
- Liao, N.-H., Xin, Y.-L., Fan, X.-L., et al. 2016, *ApJS*, 226, 17
- Lou, Z., Liang, M., Yao, D., et al. 2016, in *Society of Photo-Optical Instrumentation Engineers (SPIE) Conference Series*, Vol. 10154, Proc. SPIE, 101542A
- Madejski, G. G., & Sikora, M. 2016, *ARA&A*, 54, 725
- Marcotulli, L., Paliya, V., Ajello, M., et al. 2020, *ApJ*, 889, 164
- Masci, F. J., Laher, R. R., Rusholme, B., et al. 2019, *PASP*, 131, 018003
- Massaro, E., Giommi, P., Leto, C., et al. 2009, *A&A*, 495, 691
- Mathur, S., & Elvis, M. 1995, *AJ*, 110, 1551
- Mattox, J. R., Bertsch, D. L., Chiang, J., et al. 1996, *ApJ*, 461, 396
- McEnery, J., & Amego Team. 2020, in *American Astronomical Society Meeting Abstracts*, American Astronomical Society Meeting Abstracts, 372.15
- Moran, E. C., & Helfand, D. J. 1997, *ApJL*, 484, L95
- Nolan, P. L., Abdo, A. A., Ackermann, M., et al. 2012, *ApJS*, 199, 31

- Oh, K., Koss, M., Markwardt, C. B., et al. 2018, *ApJS*, 235, 4
- Pâris, I., Petitjean, P., Aubourg, É., et al. 2014, *A&A*, 563, A54
- Patnaik, A. R., Browne, I. W. A., Wilkinson, P. N., & Wrobel, J. M. 1992, *MNRAS*, 254, 655
- Planck Collaboration, Ade, P. A. R., Aghanim, N., et al. 2014, *A&A*, 571, A16
- Romani, R. W. 2006, *AJ*, 132, 1959
- Romani, R. W., Sowards-Emmerd, D., Greenhill, L., & Michelson, P. 2004, *ApJL*, 610, L9
- Sbarrato, T., Ghisellini, G., Nardini, M., et al. 2012, *MNRAS*, 426, L91
- Schinzel, F. K., Sokolovsky, K. V., D'Ammando, F., et al. 2011, *A&A*, 532, A150
- Schneider, D. P., Hall, P. B., Richards, G. T., et al. 2005, *AJ*, 130, 367
- Ulrich, M.-H., Maraschi, L., & Urry, C. M. 1997, *ARA&A*, 35, 445
- Volonteri, M. 2010, *A&A Rv*, 18, 279
- Yi, W.-M., Wang, F., Wu, X.-B., et al. 2014, *ApJL*, 795, L29

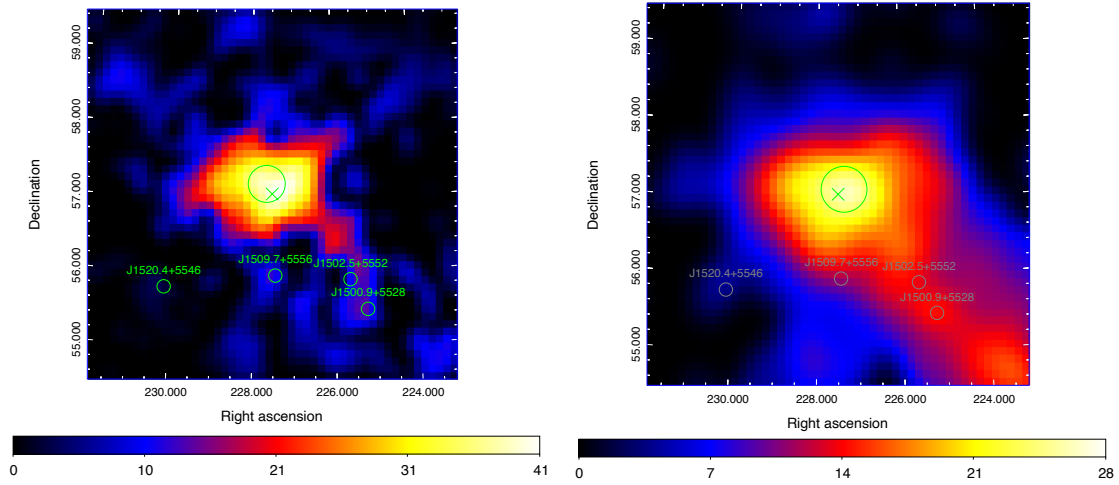


Figure 1. Residual (i.e. 4FGL J1510.1+5702 is not included in the analysis model file) TS maps for different epochs. *Left* panel: between MJD 57602 and MJD 58852; *Right* panel: between MJD 58217 and MJD 58308. The scale of the TS maps is $10^\circ \times 10^\circ$ with 0.1° per pixel. The maps are centered at 4FGL J1510.1+5702 and derived by using *Fermi*-LAT data between 0.1 and 500 GeV. The green X-shaped symbol represents the radio position of GB 1508+5714. The green circles are the 95% C. L. error radii of the locations of the γ -ray source. Locations of the nearby background sources are also marked, along with their 4FGL names. Note that their TS values are lower than 10 in the 3-month analysis, and hence they are removed from the model file, colored as grey in the right panel.

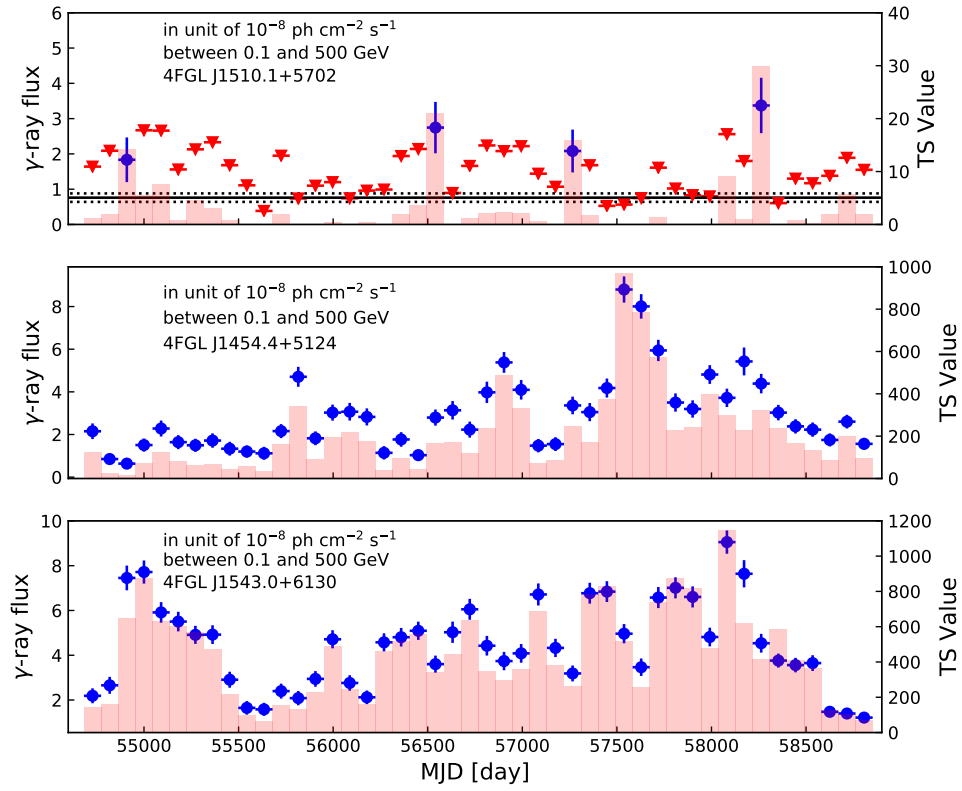


Figure 2. The 3-month time bin γ -ray light curves of the target as well as its neighbors 4FGL J1454.4+5124 and 4FGL J1543.0+6130. Blue points represent the γ -ray fluxes, while the red triangles are upper limits. Red bars are the corresponding TS values. The 11.4-year averaged γ -ray flux (solid line) and its 1σ uncertainty (dotted lines) are also marked.

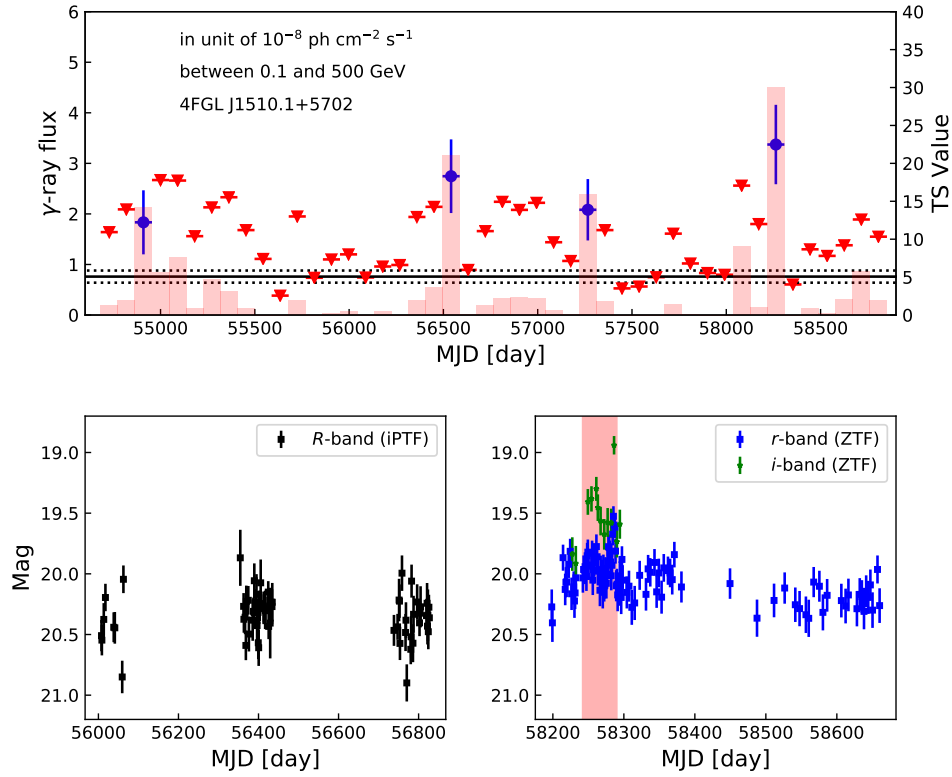


Figure 3. γ -ray and optical light curves of GB 1508+5714. *Upper panel:* as same as the upper panel of Figure 2. The red shadow area in the bottom right panel corresponds to the 48-day time epoch when TS value of the target is about 26.

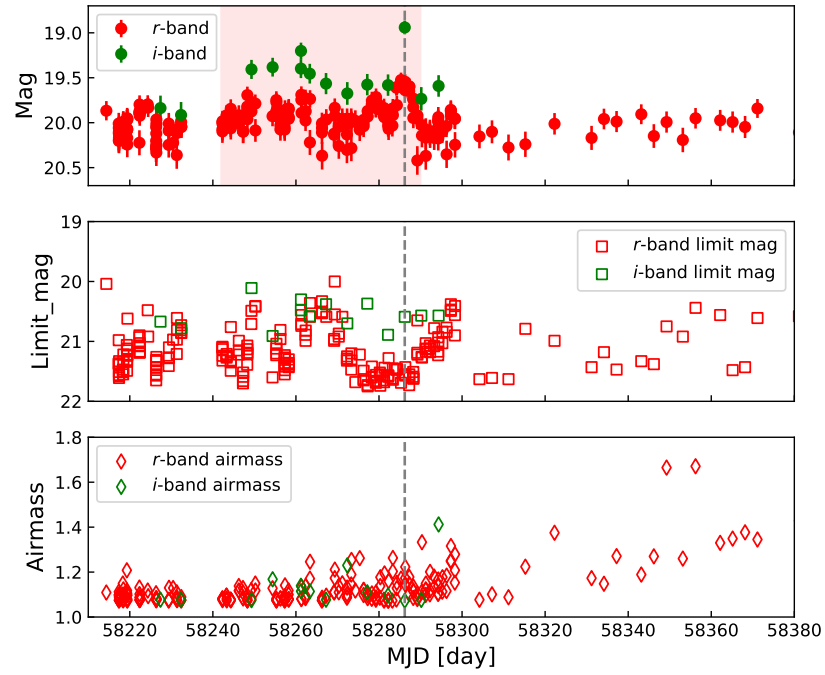


Figure 4. ZTF light curve in year 2018 with each exposure as well as the corresponding limit mag and airmass. The red shadow area represents the same 48-day time epoch that also shown in Figure 3. The vertical dashed line marks the time (i.e. MJD 58286.3) when the *i*-band flux density reaches to its peak value.